

An Outline of the Structure of $\gamma(\text{H})$ -Bismuth Molybdate, Bi_2MoO_6 , by High-Resolution Transmission Electron Microscopy

A. WATANABE,* S. HORIUCHI, AND H. KODAMA

National Institute for Research in Inorganic Materials, 1-1 Namiki, Sakura-mura, Niihari-gun, Ibaraki, 305 Japan

Received April 18, 1986; in revised form August 5, 1986

This paper gives an outline of the structure of a $\gamma(\text{H})$ form, the high-temperature stable modification of Bi_2MoO_6 polymorphs, on the basis of high-resolution transmission electron micrographs. This compound is easily quenched to room temperature and crystallizes in the space group $P2_1/c$ with $a = 17.244(1) \text{ \AA}$, $b = 22.420(2) \text{ \AA}$, $c = 5.5857(6) \text{ \AA}$, $\beta = 90.486(7)^\circ$, and $Z = 16$. The metal-atom positions have been resolved directly in $[100]$ and $[001]$ electron microscope images to show the ordering of the metal atoms. Moreover this cation framework has been based on a pseudo-face-centered cubic subcell of dimensions of about 5.6 \AA . A structural model is proposed on the assumption that the anion positions are inferred from the fluorite-related structure. Thus, bismuth has eight oxygen neighbors and each molybdenum is tetrahedrally surrounded by four oxygen atoms. © 1987 Academic Press, Inc.

Introduction

Bismuth molybdate, Bi_2MoO_6 , possesses the three polymorphs which are labeled $\gamma(\text{L})$, $\gamma(\text{H})$, and γ' : the $\gamma(\text{L})$ form is the low-temperature stable modification, the $\gamma(\text{H})$ form the high-temperature stable one, and the γ' form the metastable intermediate between them (1, 2). The $\gamma(\text{L})$ form is also known as "koechlinite" ($\mathbf{a} = 5.487 \text{ \AA}$, $\mathbf{b} = 16.226 \text{ \AA}$, $\mathbf{c} = 5.506 \text{ \AA}$; $Pca2_1$, $Z = 4$ (3)) and the refinement of structure, which consists of alternating $\text{Bi}_2\text{O}_2^{2+}$ layers and MoO_4^{2-} layers, was recently carried out using the neutron diffraction method (4, 5). On the other hand, very little is known about the structure of the $\gamma(\text{H})$ form, though the single crystal is easily obtained by flux growth (6). From a crystal chemical

standpoint or with a view to explaining the transition mechanism of Bi_2MoO_6 , a knowledge of the structure of the $\gamma(\text{H})$ form is inevitably required. We have therefore examined the structure of the $\gamma(\text{H})$ form using high-resolution transmission electron microscopy (HRTEM).

Experimental Procedure

Polycrystalline $\gamma(\text{H})\text{-Bi}_2\text{MoO}_6$ was readily prepared by solid-state techniques. The starting materials Bi_2O_3 and MoO_3 , both 99.9% pure, were thoroughly mixed in stoichiometric proportion under ethanol. After drying, the mixture was heated in a covered platinum crucible at 655°C for 40 hr. An X-ray powder diffraction (XRPD) pattern (Fig. 4) obtained with a conventional diffractometer using $\text{Cu K}\alpha$ radiation from a curved graphite monochromator agreed

* To whom correspondence should be addressed.

fairly with that reported by Chen and Smith (6) except for the relative intensities; this difference in intensities is considered in the later section. The precise lattice parameters were determined by means of the least-squares treatment (7) of 19 independent reflections in the range $2\theta = 30^\circ\text{--}100^\circ$.

Single crystals were grown using MoO_3 as a flux in the same way as described by Chen and Smith (6). A mixture of Bi_2O_3 and MoO_3 which consists of 40 mole% Bi_2O_3 was packed into a covered platinum crucible. The crucible was heated at a rate of $200^\circ\text{C hr}^{-1}$ to 950°C and then cooled at a rate of 3°C hr^{-1} to 400°C ; at this point the power was turned off. The needlelike crystals, which were transparent and homogeneously pale yellow, proved to be $\gamma(\text{H})\text{-Bi}_2\text{MoO}_6$ by the XRPD method.

HRTEM images were obtained with a Hitachi-1250 kV Type electron microscope. The needlelike single crystals were crushed in an agate mortar to yield minute fragments; subsequently, they were set on a carbon mesh supporting film. Details of the photographing conditions of the microscope were reported elsewhere (8). To confirm the observed HRTEM images, we computed the simulated images taking the dynamical scattering of electrons into consideration (9).

Results and Discussion

A series of electron diffraction photographs, two of which are inset in Fig. 1, indicated Friedel symmetry $2/m$ and the following possible reflections: hkl all orders, $h0l$ with $l = 2n$ and $0k0$ with $k = 2n$. These results uniquely determine the space group as $P2_1/c$, which agrees with that reported by Chen and Smith (6).

The precise lattice parameters determined from XRPD patterns were as follows: $\mathbf{a} = 17.244(1) \text{ \AA}$, $\mathbf{b} = 22.420(2) \text{ \AA}$, $\mathbf{c} = 5.5857(6) \text{ \AA}$, $\beta = 90.486(7)^\circ$, and $Z = 16$.

Figure 1 shows HRTEM images in the

[001] and [100] orientations. The metal atoms recognized as dark spots are arranged on the sites of a pseudo-face-centered cubic (FCC) sublattice of dimensions of about 5.6 \AA . Likewise, from XRPD patterns, Chen and Smith (6) inferred the structure based on a pseudo-FCC sublattice of about 5.6 \AA . In addition, an ordering of the metal atoms is observed; that is, the bismuth atoms aggregate to form a periodic pattern of "the Latin cross" projected on the (001) plane as shown in Figs. 3 and 5, and the atomic coordinates are given in Table I. This arrangement of metal atoms agrees well with that reported briefly by van den Elzen *et al.* (10), who gave only a section of the cation substructure inferred from the XRPD data.

In confirmation of this cation ordering, the simulated HRTEM images based on data in Table I were compared with the observed ones. As shown in Fig. 2 the best match with the observed images was obtained with crystal thicknesses of 28 \AA for [001] and 17 \AA for [100] and an objective-lens defocus of 600 \AA (underfocus).

Although the metal atoms were thus located directly by HRTEM images, the anion positions were inferred on the assumption that the structure consists of a derivative framework of fluorite-related type, each bismuth atom having eight oxygen neighbors and the molybdenum atom surrounded tetrahedrally by four oxygen neighbors. The space group $P2_1/c$ allows the following possible atomic arrangements. All atoms can fully occupy the general position $4e$: 32 Bi atoms take up 8 sets, 16 Mo atoms 4 sets, and 96 O atoms 24 sets. The oxygen positions based on the above assumption were estimated in the way that the Bi–O bond lengths range from a value of 2.5 up to 3.2 \AA and the Mo–O distances in the tetrahedra are 1.9 \AA . The positional parameters thus deduced are tabulated in Table I. An outline of the unit cell of the proposed structure is illustrated in Fig. 3. The oxygen atoms O(21)–O(24) lie exactly

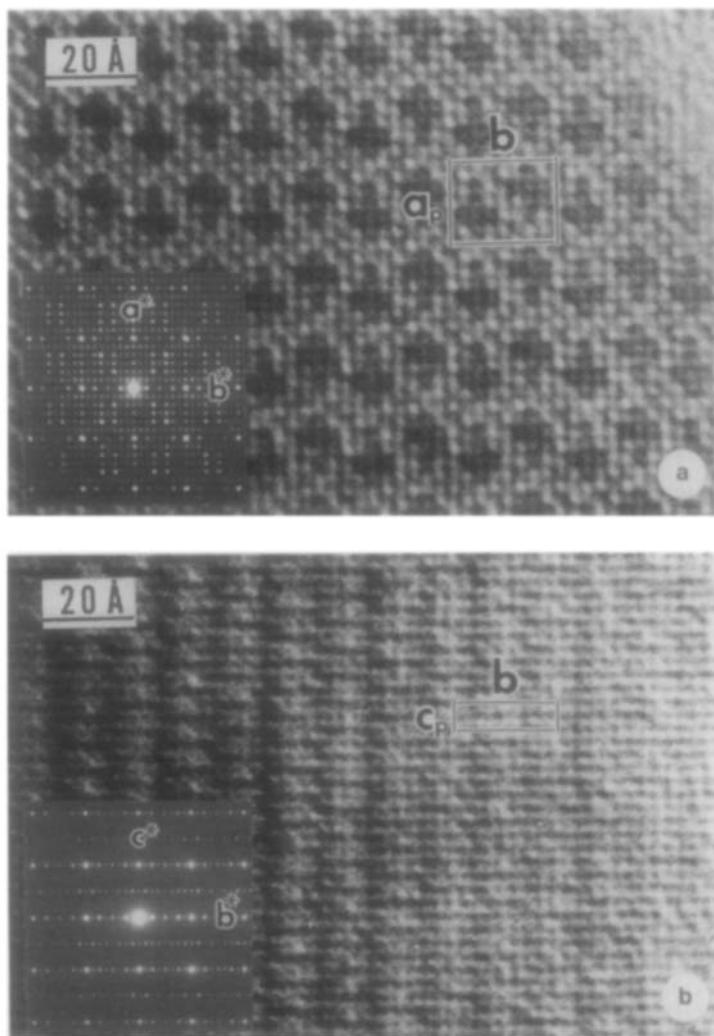


FIG. 1. HRTEM images of $\gamma(\text{H})\text{-Bi}_2\text{MoO}_6$. (a) The one in the $[001]$ orientation and (b) the one in the $[100]$ orientation. Insets: the unit-cell outline ($a_p = a \sin \beta$ and $c_p = c \sin \beta$), the corresponding electron-diffraction pattern, and the scale.

on a glide plane (c) and/or a screw axis (2_1) in this proposed structure, but they would seem to occupy positions off the translational symmetry elements in the actual structure. Furthermore, as suggested by Bode *et al.* (11), it appears likely that the molybdenum atom is coordinated by five oxygens; in other words, the coordination polyhedron would probably be an irregular

trigonal bipyramid rather than the regular tetrahedron depicted in Fig. 3.

At this point, we can further confirm the proposed structure model, specifically for the cation ordering, by calculating XRPD intensities based on the atomic coordinates in Table I and the overall temperature parameter, $B = 0.5 \text{ \AA}^2$. The results are changed to an XRPD pattern using a simulation

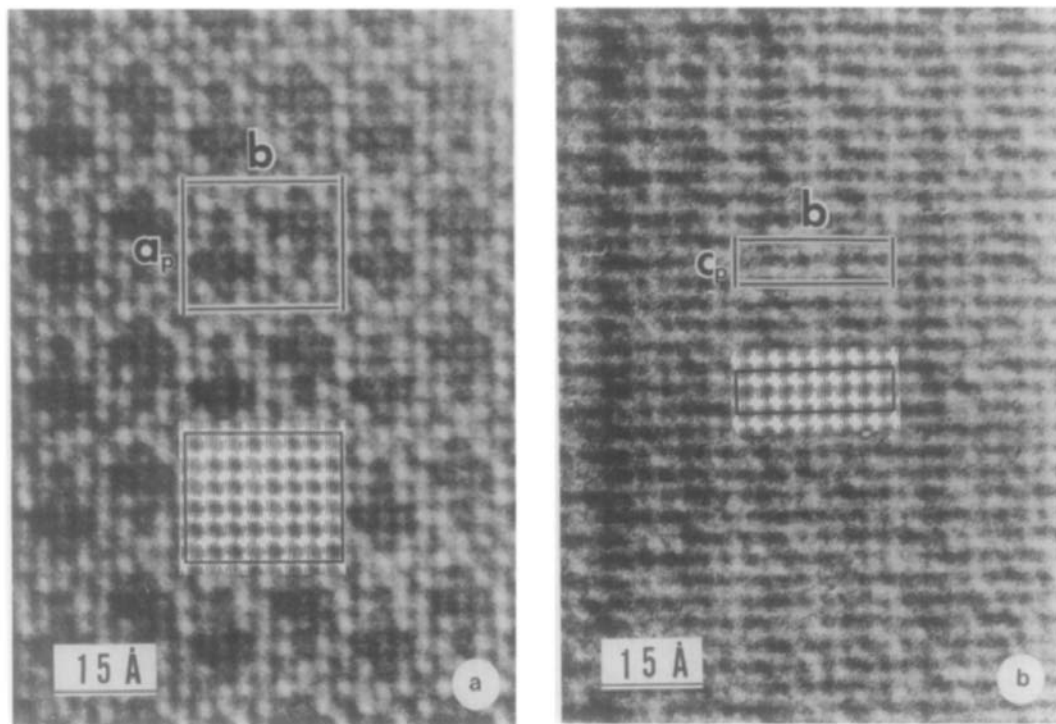


FIG. 2. Simulated images computed for the structure based on Table I, assuming crystal thicknesses of (a) 28 Å for [001] and (b) 17 Å for [100] and a 600-Å underfocus.

computer program (12) and are shown in Fig. 4 along with the observed XRPD pattern. We can see that the calculated pattern is in essential agreement with the observed XRPD one. Thus the actual structure is probably not far from the proposed one. Anyway, to determine the actual structure, especially the oxygen positions, a single crystal X-ray diffraction analysis or a neutron diffraction analysis is needed.

Chen and Smith (6) prepared γ (H)-type polycrystalline specimens by grinding lumps casted from the melt, and reported XRPD data in which the reflection 600 has the strongest relative intensity. Whereas our results gave the strongest reflection $\bar{3}41$ (corresponding to 341 by Chen and Smith (6) because of their $\beta < 90^\circ$) not only in both observed and calculated powder patterns but also in single crystal X-ray diffrac-

tion (13). This difference in the relative intensities can be explained from preferred orientation, using the proposed structure which leads to the presence of a cleavage plane. That is, as is obvious from Figs. 1 and 3, the cruciform parts consisting of bismuth and oxygen atoms are regarded as the fluorite-related structure which extends infinitely only along [001], so that the (001) plane is not a cleavage plane. On the other hand, the remaining part surrounding the cruciform ones consists mainly of isolated MoO_4 tetrahedra, and (100) and (010) planes just cut through gaps between these isolated MoO_4 tetrahedra. It would seem that these gaps are of weak-bonded portions. Consequently both (100) and (010) planes are expected to be cleavage planes; however, the (100) plane is adjacent to more MoO_4 tetrahedra than the (010). So

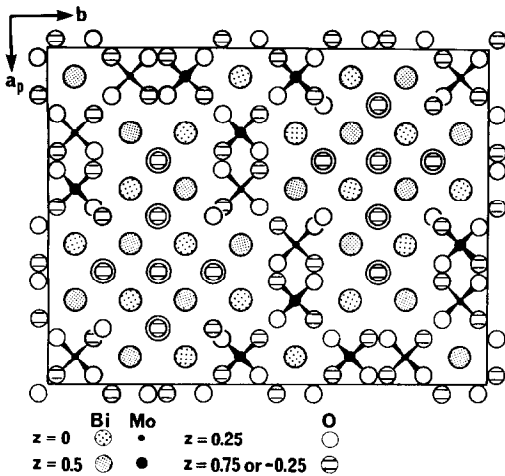


FIG. 3. The proposed structure of $\gamma(\text{H})\text{-Bi}_2\text{MoO}_6$ projected on the (001) plane. $a_p = a \sin \beta$.

the (100) plane is regarded as a cleavage plane. In fact, the relation between cleavage planes and MoO_4 tetrahedra was found in $\text{Bi}_2(\text{MoO}_4)_3$ (14), in which cation (Bi^{3+}) vacancies and some MoO_4 tetrahedra are concentrated in planes parallel to the (100) to result in a cleavage plane. Considering the presence of the cleavage plane in $\gamma(\text{H})\text{-Bi}_2\text{MoO}_6$, the relative intensities depend primarily upon the conditions of sample preparation, especially upon a firing temperature, because an excessive grain growth during solid-state reaction and subsequent pulverization which tends to split the grains along the cleavage planes lead to a great many ($h00$) planes. Actually, in polycrystalline sample preparation of $\gamma(\text{H})\text{-Bi}_2\text{MoO}_6$ by solid-state techniques, the higher the firing temperatures, the stronger the relative intensities of $h00$, particularly 600. Even at a relatively low temperature of 650°C , a heat treatment longer than 100 hr eventually brings preferred orientation of ($h00$).

The $\gamma(\text{L})$ form transforms irreversibly to the $\gamma(\text{H})$ form via the metastable γ'' form under atmospheric pressure (1). Also the

structure of the γ'' form is not analyzed because of its metastable, nonquenchable nature. Nevertheless, since the enthalpy of the $\gamma(\text{L}) \rightarrow \gamma''$ transition is too small (about $0.1 \text{ kcal mole}^{-1}$ (1)) for a reconstructive transition, the structure of the γ'' form will probably resemble that of the $\gamma(\text{L})$ form. Thus, we can easily understand the irre-

TABLE I
PROPOSED ATOMIC
COORDINATES FOR
 $\gamma(\text{H})\text{-Bi}_2\text{MoO}_6$

Atom	x	y	z
Mo(1)	$\frac{1}{12}$	$\frac{3}{16}$	0
Mo(2)	$\frac{3}{12}$	$\frac{1}{16}$	0
Mo(3)	$\frac{5}{12}$	$\frac{1}{16}$	$\frac{1}{2}$
Mo(4)	$\frac{11}{12}$	$\frac{1}{16}$	0
Bi(1)	$\frac{1}{12}$	$\frac{1}{16}$	$\frac{1}{2}$
Bi(2)	$\frac{3}{12}$	$\frac{3}{16}$	$\frac{1}{2}$
Bi(3)	$\frac{5}{12}$	$\frac{1}{16}$	0
Bi(4)	$\frac{7}{12}$	$\frac{1}{16}$	0
Bi(5)	$\frac{9}{12}$	$\frac{3}{16}$	$\frac{1}{2}$
Bi(6)	$\frac{11}{12}$	$\frac{1}{16}$	$\frac{1}{2}$
Bi(7)	$\frac{1}{12}$	$\frac{3}{16}$	0
Bi(8)	$\frac{11}{12}$	$\frac{1}{16}$	$\frac{1}{2}$
O(1)	$\frac{1}{30}$	$\frac{3}{20}$	$\frac{1}{4}$
O(2)	$\frac{3}{30}$	$\frac{3}{20}$	$\frac{1}{4}$
O(3)	$\frac{5}{30}$	$\frac{1}{20}$	$\frac{3}{4}$
O(4)	$\frac{7}{30}$	$\frac{3}{20}$	$\frac{3}{4}$
O(5)	$\frac{9}{30}$	$\frac{1}{20}$	$\frac{1}{4}$
O(6)	$\frac{11}{30}$	$\frac{3}{20}$	$\frac{1}{4}$
O(7)	$\frac{1}{30}$	$\frac{13}{20}$	$\frac{3}{4}$
O(8)	$\frac{3}{30}$	$\frac{1}{20}$	$\frac{3}{4}$
O(9)	$\frac{5}{30}$	$\frac{1}{20}$	$\frac{1}{4}$
O(10)	$\frac{7}{30}$	$\frac{3}{20}$	$\frac{1}{4}$
O(11)	$\frac{9}{30}$	$\frac{1}{20}$	$\frac{3}{4}$
O(12)	$\frac{11}{30}$	$\frac{1}{20}$	$\frac{3}{4}$
O(13)	$\frac{13}{30}$	$\frac{3}{20}$	$\frac{1}{4}$
O(14)	$\frac{15}{30}$	$\frac{1}{20}$	$\frac{1}{4}$
O(15)	$\frac{17}{30}$	$\frac{1}{20}$	$\frac{3}{4}$
O(16)	$\frac{19}{30}$	$\frac{3}{20}$	$\frac{3}{4}$
O(17)	$\frac{21}{30}$	$\frac{5}{20}$	$\frac{3}{4}$
O(18)	$\frac{23}{30}$	$\frac{5}{20}$	$\frac{1}{4}$
O(19)	$\frac{25}{30}$	$\frac{3}{20}$	$\frac{3}{4}$
O(20)	$\frac{27}{30}$	$\frac{1}{20}$	$\frac{1}{4}$
O(21)	$\frac{29}{30}$	$\frac{13}{20}$	$\frac{1}{4}$
O(22)	$\frac{1}{30}$	$\frac{13}{20}$	$\frac{1}{4}$
O(23)	$\frac{3}{30}$	$\frac{13}{20}$	$\frac{1}{4}$
O(24)	$\frac{5}{30}$	$\frac{13}{20}$	$\frac{3}{4}$

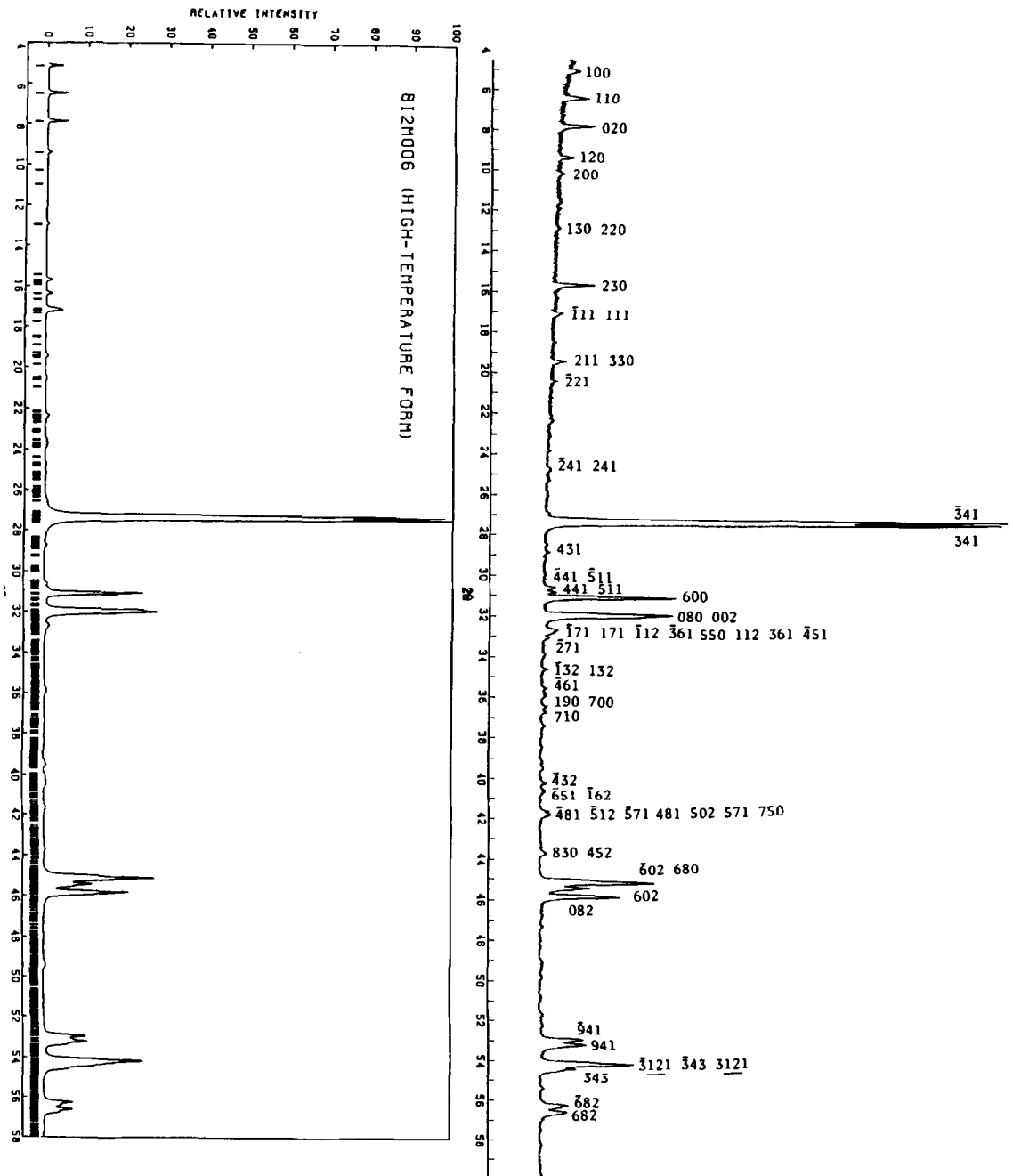


FIG. 4. The observed and calculated powder diffraction patterns for $\gamma(H)\text{-Bi}_2\text{MoO}_6$. The right curve is the observed pattern which was measured by $\text{Cu K}\alpha$ (45 kV/30 mA) radiation from a curved graphite monochromator. The left curve is the calculated one; the short vertical lines indicate the positions of possible Bragg reflections of $\text{Cu K}\alpha_1$ and $\text{Cu K}\alpha_2$.

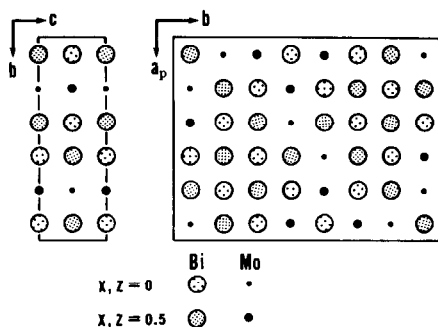


FIG. 5. Structural relationship between $\gamma(\text{L})\text{-Bi}_2\text{MoO}_6$ and $\gamma(\text{H})\text{-Bi}_2\text{MoO}_6$. The left is the projection of idealized $\gamma(\text{L})\text{-Bi}_2\text{MoO}_6$ on (100) and the right the projection of $\gamma(\text{H})\text{-Bi}_2\text{MoO}_6$ on (001). The oxygen atoms are not shown.

versibility making a comparison between $\gamma(\text{L})$ and $\gamma(\text{H})$ structures shown in Fig. 5; a considerable reconstruction is seen in cation substructure. From the unit cell dimensions of $\gamma(\text{L})$ and $\gamma(\text{H})$ forms, the topotactic relations may be roughly deduced as follows: $a_{\gamma(\text{H})} \approx b_{\gamma(\text{L})}$, $b_{\gamma(\text{H})} \approx 4c_{\gamma(\text{L})}$, and $c_{\gamma(\text{H})} \approx a_{\gamma(\text{L})}$. To date, however, there is no sufficient evidence to warrant these relations. So the explanation of the transition mechanism including the structural refinement of the $\gamma(\text{H})$ form and the topotactic relations will be the subject of future studies.

Acknowledgment

The authors are indebted to Dr. F. Izumi for the computer calculation of XRPD patterns.

References

1. A. WATANABE AND H. KODAMA, *J. Solid State Chem.* **35**, 240 (1980).
2. H. KODAMA AND A. WATANABE, *J. Solid State Chem.* **56**, 225 (1985).
3. A. F. VAN DEN ELZEN AND G. D. RIECK, *Acta Crystallogr., Sect. B* **29**, 2436 (1973).
4. F. THEOBALD, A. LAARIF, AND A. W. HEWAT, *Ferroelectrics* **56**, 219 (1984).
5. R. G. TELLER, J. F. BRAZDIL, R. K. GRASSELLI, AND J. D. JORGENSEN, *Acta Crystallogr., Sect. C* **40**, 2001 (1984).
6. TU. CHEN AND G. S. SMITH, *J. Solid State Chem.* **13**, 288 (1975).
7. D. E. APPLEMAN AND H. T. EVANS, JR., National Technical Information Service PB-216, 188 (1973).
8. S. HORIUCHI, *Ultramicroscopy* **10**, 229 (1982).
9. J. M. COWLEY AND A. F. MOODIE, *Acta Crystallogr.* **10**, 609 (1957).
10. A. F. VAN DEN ELZEN, L. BOON, AND R. METSELAAR, "Solid State Chemistry 1982" (R. Metselaar, H. J. M. Heijligers, and J. Schoonman, Eds.), pp. 773-776, Elsevier, Amsterdam (1983).
11. J. H. G. BODE, H. R. KUIJT, M. A. J. TH. LAHEY, AND G. BLASSE, *J. Solid State Chem.* **8**, 114 (1973).
12. F. IZUMI, *J. Crystallogr. Soc. Japan* **17**, 37 (1985).
13. N. ISHIZAWA, private communication (1985).
14. A. F. VAN DEN ELZEN AND G. D. RIECK, *Acta Crystallogr., Sect. B* **29**, 2433 (1973).